11-2023

Subseasonal Clustering of Atmospheric rivers over the western United States

Emily Slinskey
University of California Los Angeles

Paul Loikith
Portland State University, ploikith@pdx.edu

Naomi Goldenson
University of California Los Angeles

Jesse Norris
Scripps Institution of Oceanography

Jesse Hall
University of California Los Angeles

Citation Details

Slinskey, E. A., Hall, A., Goldenson, N., Loikith, P. C., & Norris, J. (2023). Subseasonal clustering of atmospheric rivers over the western United States. Journal of Geophysical Research: Atmospheres, 128(22), e2023JD038833.

JGR Atmospheres

RESEARCH ARTICLE
10.1029/2023JD038833

Subseasonal Clustering of Atmospheric Rivers Over the Western United States

Emily A. Slinskey[1], Alex Hall[1], Naomi Goldenson[1], Paul C. Loikith[2], and Jesse Norris[1]

[1]Atmospheric and Oceanic Sciences, University of California Los Angeles, Los Angeles, CA, USA, [2]Geography, Portland State University, Portland, OR, USA

Key Points:

- Atmospheric rivers (ARs) temporally cluster at a greater-than-random rate across the western United States (US) with a distinct geographical pattern
- Compared to the Northwest, Southwest clusters are longer-lived, consist of more ARs and account for a larger fraction of total AR occurrence
- A considerable fraction of western US total and extreme hourly precipitation is attributable to AR clusters

Supporting Information:

Supporting Information may be found in the online version of this article.

Correspondence to:

E. A. Slinskey,
eslinskey@g.ucla.edu

Citation:

Slinskey, E. A., Hall, A., Goldenson, N., Loikith, P. C., & Norris, J. (2023). Subseasonal clustering of atmospheric rivers over the western United States. *Journal of Geophysical Research: Atmospheres*, *128*, e2023JD038833. https://doi.org/10.1029/2023JD038833

Received 7 MAR 2023
Accepted 22 OCT 2023

Abstract The serial occurrence of atmospheric rivers (ARs) along the US West Coast can lead to prolonged and exacerbated hydrologic impacts, threatening flood-control and water-supply infrastructure due to soil saturation and diminished recovery time between storms. Here a statistical approach for quantifying subseasonal temporal clustering among extreme events is applied to a 41-year (1979–2019) wintertime AR catalog across the western United States (US). Observed AR occurrence, compared against a randomly distributed AR timeseries with the same average event density, reveals temporal clustering at a greater-than-random rate across the western US with a distinct geographical pattern. Compared to the Pacific Northwest, significant AR clusters over the northern Coastal Range of California and Sierra Nevada are more frequent and occur over longer time periods. Clusters along the California Coastal Range typically persist for 2 weeks, are composed of 4–5 ARs per cluster, and account for over 85% of total AR occurrence. Across the northwest Coast-Cascade Ranges, clusters account for ~50% of total AR occurrence, typically last 8–10 days, and contain 3–4 individual AR events. Based on precipitation data from a high-resolution dynamical downscaling of reanalysis, the fractions of total and extreme hourly precipitation attributable to AR clusters are largest along the northern California coast and in the Sierra Nevada. Interannual variability among clusters highlights their importance for determining whether a particular water year is anomalously wet or dry. The mechanisms behind this unusual clustering are unclear and require further research.

Plain Language Summary Atmospheric rivers, or long narrow regions of enhanced water vapor transport, are an important component of the midlatitude water cycle, responsible for producing precipitation and associated extremes. Atmospheric rivers occurring close in time or one after another can lead to exaggerated impacts due to the decreased time between periods of precipitation. Based on the historical record, we identify the timescales at which wintertime atmospheric rivers cluster at a rate different from what would be expected by random chance over the western United States. Compared to the Pacific Northwest, atmospheric river clusters over the mountainous regions of California occur more frequently, over longer periods of time, and account for a larger proportion of total atmospheric river occurrence. Atmospheric rivers in this region are also responsible for a large fraction of total precipitation and are commonly associated with precipitation extremes. The year-to-year occurrence of clusters is important for determining wet versus dry years. Future work will identify the atmospheric patterns behind atmospheric river clustering over different geographies.

1. Introduction

The impacts of extreme weather and climate events can become amplified when occurring in close temporal proximity or succession. Compound extreme events continue to emerge as a growing and active area of research arising from complex interactions between multiple physical drivers and land-surface impacts, resulting in significant societal and/or environmental impacts (Zscheischler et al., 2018, 2020). Of particular concern are temporally compounding events, occurring as a succession of events at a given location. These may be of the same type (e.g., consecutive extreme precipitation events) or different (e.g., a tropical cyclone followed by a heatwave). Temporally compounding events have the potential to overwhelm natural and human systems, maximizing ecological and societal vulnerabilities due to diminished recovery time between impacts.

Drivers and impacts associated with temporally compounding events have been studied extensively for extratropical cyclones (ETCs) (Mailier et al., 2006; Pinto et al., 2014) and precipitation extremes (Barton et al., 2016; Kopp et al., 2021; Tuel & Martius, 2021a, 2021b, 2022). Sequences of cyclones are often linked to secondary cyclogenesis along trailing fronts, Rossby wave packets, and/or persistent favorable jet states (Dacre & Pinto, 2020).

Influenced by large-scale teleconnection patterns, tropical forcing, and persistent atmospheric circulation patterns, cyclone clusters can lead to large socioeconomic impacts and cumulative losses (Vitolo et al., 2009). Similarly, due to an increased risk of flooding and landslides, clustering among extreme precipitation events has been examined (e.g., Martius et al., 2013; Priestley et al., 2017) and linked to patterns of upper-level Rossby wave breaking (Barton et al., 2016). The presence of clustering among these events also implies the periodic prolonged absence of precipitation, with associated impacts on water supply.

Various methodologies have been used to investigate temporal clustering. Of the most common are relative frequency metrics, involving a comparison between the variability in event occurrence to a mean or expected value of occurrence. Villarini et al. (2011) conducted a systematic analysis of extreme precipitation clustering annually across the midwestern US using a dispersion coefficient based on the variance-to-mean ratio of annual extreme counts. Using a point-process approach to quantify variability among monthly cyclone counts, Mailier et al. (2006) found statistically significant overdispersion among extratropical cyclone clusters affecting western Europe, implying more serial clustering than would be expected by chance. In both cases, homogeneous Poisson point processes were used to provide a frame of reference following assumptions of stationarity and independence among events. Here, a similar approach is applied to quantify subseasonal temporal clustering among atmospheric river (AR) events across the western United States (US).

ARs are long, narrow corridors of enhanced water vapor transport in the lower troposphere (Zhu & Newell, 1998). Responsible for delivering large amounts of water to the western US, often related to flooding (e.g., Corringham et al., 2019), ARs are critical for determining the hydroclimate in the midlatitudes and poleward flank of the subtropics. Often related to the low-level convergence within extratropical cyclones, ARs are modulated by extratropical dynamics through Rossby wave propagation and breaking (Payne & Magnusdottir, 2014). Favorable and unfavorable conditions for AR activity are further sensitive to large-scale modes of climate variability (Guirguis et al., 2018). Their interactive relationship within this larger, synoptic-scale dynamical system presents potential implications on frequency patterns (i.e., interannual variability) and storm intensity, as well as the severity of associated hydrologic impacts.

As an emerging area of research (e.g., Fish et al., 2019, 2022), AR sequences have garnered significant attention due to their large cumulative impacts (e.g., 2017 Oroville Dam Crisis; White et al., 2019) and potential for generating megaflood conditions (Huang & Swain, 2022). Several case study analyses have examined the impacts of multiple sequential ARs (e.g., Cordeira et al., 2013; Dominguez et al., 2018; Michaelis et al., 2022; White et al., 2019) which often generate increased precipitation totals and elevated stream discharge rates compared to isolated ARs (Vano et al., 2018). Within the historical record, one of the most notable successive AR events occurred in the winter of 1861/1862, generating intense precipitation in Northern California over 43 days, capped by a warm storm event that produced catastrophic flooding over the Sacramento Valley (Dettinger & Ingram, 2013; Null & Hulbert, 2007). This precedent-setting event prompted the ARkStorm scenario, a hypothetical storm intended to provide emergency responders, resource managers, and the public with a realistic assessment of the very real threat to human life, property, and ecosystems posed by extreme successive AR events along the West Coast (Porter et al., 2011). Extended periods of AR conditions are often accompanied by greater moisture content than less persistent ARs, enhancing the potential for hydrologic impacts. Storm duration has been shown to be a strong indicator for precipitation and streamflow magnitude (Lamjiri et al., 2017; Ralph et al., 2013, 2019). Understanding changing patterns in AR sequencing over space and time, therefore, has important implications for forecasting applications associated with water availability and/or flood potential.

Recently, Fish et al. (2019) introduced the concept of AR families based on a single-point analysis using a 13-year data set of AR conditions observed at the Bodega Bay AR Observatory in Northern California. They found that ARs occurring within 120 hr of another exhibit distinct large-scale characteristics from those occurring in greater isolation. These synoptic environments are often characterized by lower geopotential heights throughout the North Pacific, an enhanced subtropical high, and a strong zonal North Pacific jet. A follow-on analysis, Fish et al. (2022), further linked AR families with specific phases of El Niño Southern Oscillation and the Madden-Julian Oscillation, pointing to the potential seasonal-to-subseasonal predictability of such events. This work suggests that ARs cluster in time under certain synoptic regimes useful for improving situational awareness and forecasting capabilities, yet synoptic atmospheric variability can produce weather sequences whose features (such as ARs) occur in sequence purely by chance. Thus, it remains unclear whether the ARs in the AR families are associated by chance or whether there is a mechanism that causes ARs to "stick" together. It also remains

to be determined whether and how AR clustering varies geographically along the pronounced meridional precipitation gradient stretching from Baja California to southwestern Canada.

Here a statistical framework to objectively identify subseasonal temporal clustering among AR events is applied to a reanalysis-based, 41-year, hourly AR catalog across the western US. A seasonal climatology of AR clusters, defined as temporal clustering beyond what would be expected by random chance, is presented to quantify their climatological characteristics (frequency, duration, and influence on precipitation). Here, clustering is investigated as a function of geographical location and is not dependent on the clustering time scales of other phenomena (i.e., ETC's) as in Fish et al., 2019. To improve the understanding of associated cumulative impacts, significant AR clusters are further linked to precipitation characteristics using a high-resolution, dynamically downscaled reanalysis product. Results aim to serve as a benchmark for measuring future change in AR cluster characteristics and associated precipitation under warming as well as provide a target for a global/regional climate- and/or weather predication model evaluation.

2. Data and Methodology

2.1. Data

2.1.1. Atmospheric Rivers

ARs are identified in the European Centre for Medium-range Weather Forecasting's Reanalysis v5 (ERA5; Hersbach et al., 2020) product for 1979–2019 at a $1° \times 1°$ spatial resolution and hourly temporal resolution using an objective AR identification algorithm (Guan & Waliser, 2015; updated in Guan et al., 2018). The approach uses multiple sequentially higher IVT magnitude percentile-based thresholds (i.e., 85–95th percentile and fixed 100 kg m^{-1} s^{-1} lower limit) to identify contiguous areas of connected grid points or "objects." Objects are further filtered based on criteria for IVT direction (within 45° of the shape orientation with an appreciable poleward component of >50 kg m^{-1} s^{-1}), length (>2,000 km), and length/width ratio (>2).

2.1.2. Precipitation

Precipitation estimates from a dynamically downscaled reanalysis product are used to link with detected ARs. This product is a downscaling of ERA5 over the western US by the Weather Research and Forecasting (WRF) model on a 9-km grid with hourly output (ERA5-WRF; Rahimi et al., 2022). Compared to ERA5, ERA5-WRF has been shown to better represent orographic precipitation across the western US, as well as the timing and magnitude of AR-driven precipitation (Rahimi et al., 2022). A minimum distance-based interpolation scheme is used to link AR timesteps in ERA5 to precipitation in ERA5-WRF (as in Slinskey et al., 2020). This approach assigns the coarser resolution grid points to the finer resolution grid points with the shortest distance from the grid cell center.

2.2. Methodology

2.2.1. Defining ARs

Discrete AR events are isolated from the Guan and Waliser hourly AR catalog. First, AR conditions separated by ≤6 hr are considered a continuous event. AR events then require at least eight consecutive hours of AR conditions over a given location, following Ralph et al. (2013). A sensitivity analysis examining the influence of applying 12 and 24 hr minimum AR event duration thresholds on average AR cluster frequency and duration is provided in Figure S1 in Supporting Information S1. Results are minimally sensitive to the use of a 12 hr threshold, while a 24 hr minimum produces less spatial heterogeneity in the metrics domain wide. The 8 hr threshold is retained as it allows for shorter-duration AR events to be included as a part of cluster which may contribute to impacts via a cascading effect within an AR sequence.

Here, we focus on AR events across the heart of the western US wet season, defined as December, January, February (DJF), due to its relevance for impacts, including precipitation extremes and associated flooding. However, we note that ARs can occur outside of these months, especially over the northern half of our study domain (Slinskey et al., 2020). AR event frequency, based on the above criteria, is characterized by a maximum (>11 events/season) along the Oregon-Washington border stretching into the Olympic Peninsula as well as along the northern Coastal Range of California (Figure 1a). AR events are less frequent (<7 events/season) across Southern California and the interior following a negative southeastward gradient across the domain.

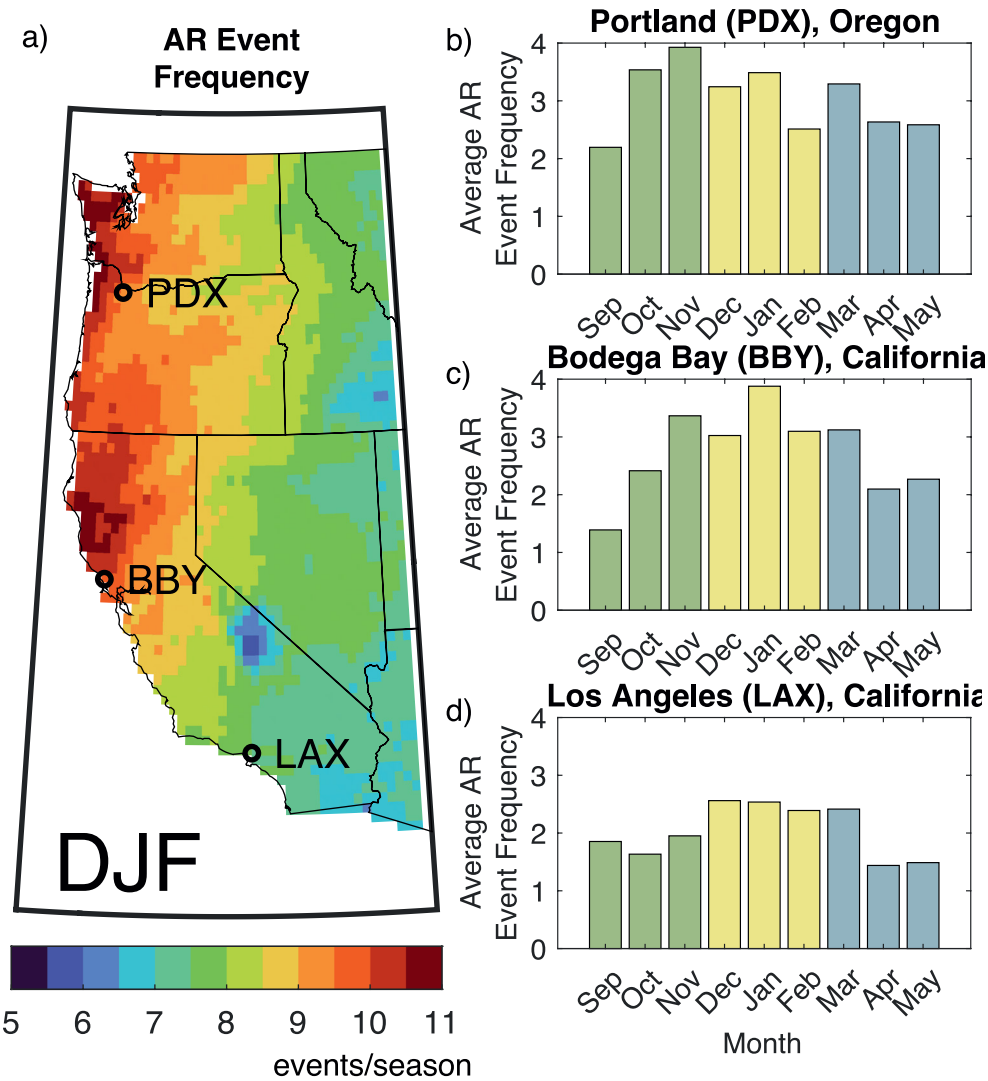

Figure 1. (a) AR event frequency (shading) is shown as events per season. Results are shown for December, January, February (DJF) at each grid point based on ARs identified between 1979 and 2019. Histograms of AR event frequency by month at (b) Portland, Oregon, (c) Bodega Bay, California, and (d) Los Angeles, California.

2.2.2. Quantifying the Subseasonal Temporal Clustering of ARs

The serial clustering of ARs refers to the passage of multiple AR events over a fixed location (i.e., grid point) within a given period-of-time. With the intention of focusing on clustering over longer timescales (i.e., weekly to monthly), the hourly timeseries of AR event occurrence is first filtered to disregard all AR timesteps except the first of each event (Barton et al., 2016). The outcome is a binary timeseries of AR events in which the first hour of each event is retained as the representative timestep.

The Ripley's K Function (Ripley, 1981) is used to quantify subseasonal clustering among AR events within the timeseries. The approach can be understood as the average number of events (i.e., ARs) that occur within time t centered around a randomly chosen event in the timeseries. Mathematically, K is estimated as

$$\hat{K}(t) = \frac{1}{n}\sum_{i=1}^{n}\sum_{j\neq i} I_{|t_i - t_j| \leq t},$$

where n is the total number of events, t_i is the time of an event, and t_j are the times of all other events in the same season as t_i. The sum of the indicator function,

$$I_{|t_i - t_j| \leq t} = \begin{cases} 1 & \text{if} |t_i - t_j| \leq t \\ 0 & \text{if} \, |t_i - t_j| > t \end{cases}$$

increases as more events occur within time t, referred to as the aggregation period, before and after a given event in the timeseries. In other words, for a given event, all other events occurring within a set time period (i.e., aggregation period) are tallied and normalized by the total number of events in the timeseries. In turn, this statistical approach provides information about the tendency toward temporal clustering in the timeseries, such that the larger the value of $\hat{K}$ for a given aggregation period (t), the more clustered the events. The cumulative nature of the function allows clustering at shorter timescales to contribute to clustering at longer timescales.

Significance is determined at each grid point through a comparison between the empirical Ripley's $\hat{K}$ values and those obtained from a Monte Carlo sample of 1,000 simulated homogeneous Poisson processes with the same average event density as the observed series. Homogeneous Poisson processes assume events occur independently from each other at a constant rate, exhibiting complete temporal randomness with clustering only occurring by chance. Several studies have utilized this technique for testing the significance of clustering among ETCs (Mailier et al., 2006; Vitolo et al., 2009) and extreme precipitation events (Barton et al., 2016; Tuel & Martius, 2021a, 2021b; Villarini et al., 2011).

A false detection rate procedure (Wilks, 2016) with a baseline significance level of 5% is implemented to identify aggregation periods with statistically significant clustering as in Tuel and Martius (2021a, 2021b). For a given aggregation period, an empirical p-value for the observed K is defined as one minus its percentile rank in the corresponding Monte-Carlo sample. For example, an observed K larger than all the K values in the Monte-Carlo sample would have a p-value of zero. A lower p-value, therefore, corresponds to a higher K-value. The observed series is said to exhibit a significant temporal clustering pattern if its p-value is lower than p^*, expressed as

$$p^* = \max_i \left(p_i \leq \frac{i}{N} \alpha \right)$$

where p_i refers to the sorted p-values from all N Monte-Carlo simulations (i.e., 1,000) and α is the chosen significance level (i.e., $\alpha = 0.05$).

All calculations are computed at each grid point across each DJF season individually. Histograms of AR event frequency by month for three locations along the West Coast show little month-to-month variation within DJF (Figures 1b and 1c). Sensitivity testing (not shown) revealed no change in the overall timescales with significant clustering for alternate definitions of the winter season (NDJF, DJF, and DJFM).

For simplicity, Ripley's K results are summarized over 10 aggregation periods ranging from 1 to 50 days at 5-day intervals (i.e., 1–5, 6–10, 11–15, etc.). Clustering is considered significant for a given t (i.e., individual aggregation period) if at least half the years (i.e., >20 years) exhibit significant clustering at that t. Significance for a given 5-day aggregation period interval is assigned if the majority of t values (i.e., >2) within that interval are significant.

2.2.3. Identification of AR Clusters

The Ripley's K function provides information about the tendency toward temporal clustering across different timescales. It does not directly identify clusters within the seasonal timeseries. To identify AR clusters, the AR event timeseries, described in Section 2.2.1, is filtered to establish AR event strings (i.e., series of AR events) in which each individual event must occur within 10 days of the previous event. Gap length criteria (i.e., ≤10-day threshold) was chosen based on a sensitivity analysis evaluating gap lengths spanning 2–24 days. The ratio of ARs meeting the gap length criteria relative to the total AR count levels off at around the 10-day period (see Figure S2 in Supporting Information S1). The length of time from the first timestep of the first event in the string to the first timestep of the last event in the string is checked against the significant aggregation periods defined at each grid point. Only strings occurring over statistically significant aggregation periods are retained for subsequent analysis. Resulting AR clusters refer to two or more AR events, in which each event occurs ≤10 days apart over a statistically significant aggregation period as defined by the Ripley's K analysis.

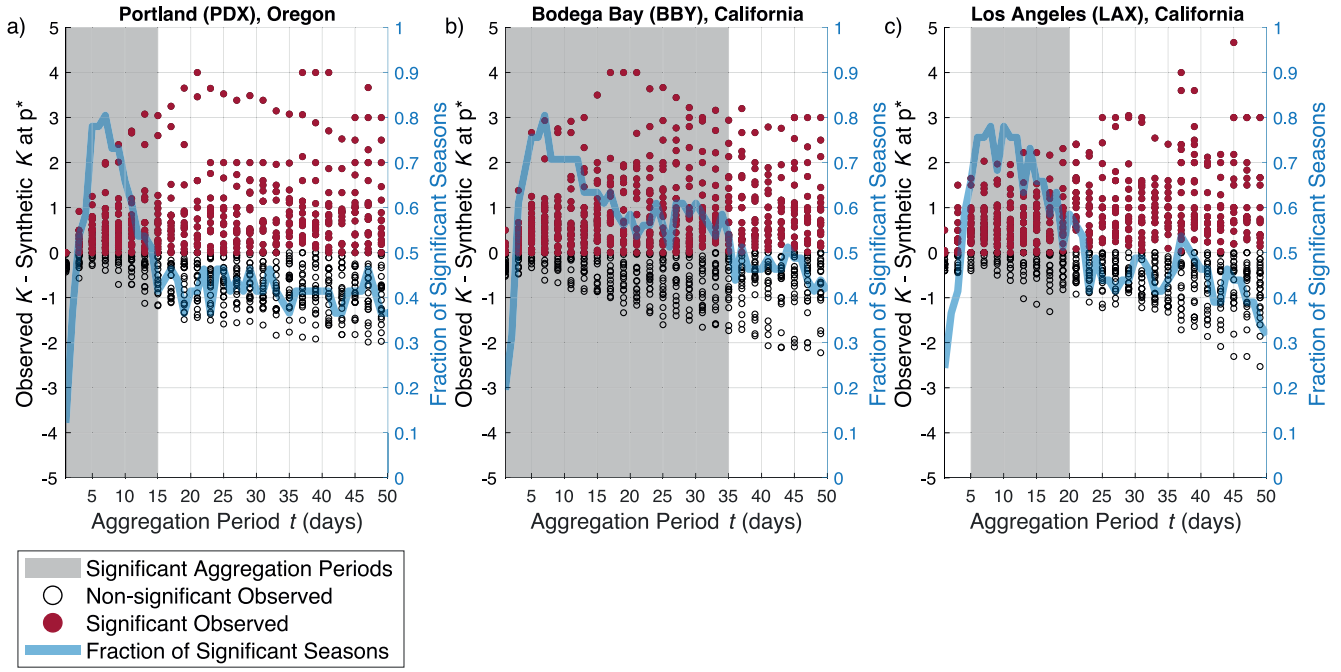

Figure 2. Ripley's K values for (a) Portland, Oregon; (b) Bodega Bay, California; and (c) Los Angeles, California for DJF. Circles represent difference between the observed K-value and synthetic K-value at p^* (y-axis) computed for each year (1979–2019) for each aggregation period (x-axis). Red filled circles represent years with significant clustering patterns based on exceedance of p*. Gray shading reflects aggregation periods with significance. The fraction of seasons with significance (blue line) is shown for each aggregation period.

Case study analyses presented in Section 3.2 illustrate examples of seasons with statistically significant AR clustering. The chosen years have documented hydrologic significance and a high ratio of clustered ARs to total ARs. Latitudinally distinct locations provide additional insight into how clustering characteristics vary geographically.

3. Results

3.1. Significant AR Clustering Timescales

The observed and simulated Ripley's K output for three representative locations along the West Coast, illustrate variability in the range of significant clustering timescales (Figure 2). The difference between the observed K and synthetic K at the 5% significance level across aggregation periods is shown for each winter season between 1979 and 2019. Positive values (red circles) along the y-axis therefore reflect a higher degree of observed clustering relative to the random series. Unshaded circles with a negative difference, represent individual winter seasons when the observed clustering characteristics did not meet the significance criteria. Significance for a particular aggregation period (gray shading) requires the fraction of significant seasons (blue line) be ≥0.5 for the majority of the 5-day interval (x-axis).

Statistically significant clustering occurs over timescales ranging from 1 to 15 days at Portland (PDX), Oregon (Figure 2a). The peak in the fraction of seasons with significance is positioned between the 5-10-day aggregation periods, with a value of 0.8. This indicates that 80% of the 41 seasons showed statistically significant clustering over these timescales. Beyond 15 days, the fraction of significant seasons is ∼0.4, meaning that significant clustering is common at longer timescales but falls just short of the 50% requirement. At Bodega Bay (BBY), California, significant clustering tends to occur over a wider range of timescales compared to PDX, extending from 1 to 35 days (Figure 2b). Like PDX, the fraction of significant seasons at BBY peaks around the 7-day aggregation period at 0.8. At Los Angeles (LAX), California, significant clustering extends from the 5 to 20-day aggregation periods (Figure 2c). The fraction of significant seasons is characterized by two peaks at 8 and 10-days, with values just shy of 0.8. After 20 days, the fraction hovers between 0.4 and 0.5. All three locations therefore reveal greater-than-random AR clustering patterns with variability in the range of significant aggregation periods. Significant clustering is limited to shorter timescales at PDX and LAX but occurs over a wider range

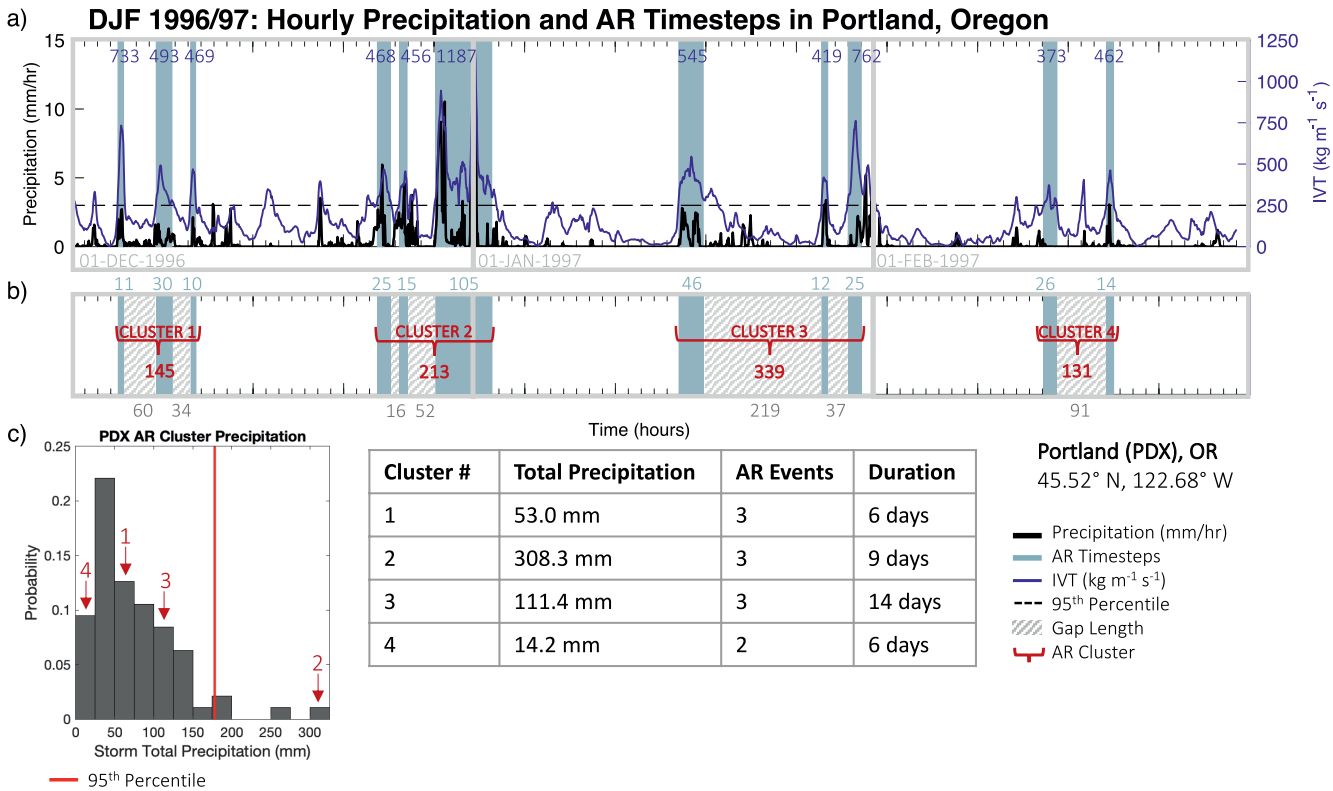

Cluster #	Total Precipitation	AR Events	Duration
1	53.0 mm	3	6 days
2	308.3 mm	3	9 days
3	111.4 mm	3	14 days
4	14.2 mm	2	6 days

Figure 3. (a) Hourly precipitation (black line; mm/hr), integrated water vapor transport (IVT; blue line; kg m^{-1} s^{-1}) and identified AR events (pale blue shading) between December 1996 and February 1997, (top panel) recorded at Portland, Oregon. Each AR event is labeled with maximum hourly IVT as a measure of AR intensity. Dashed black line signifies 95th percentile hourly precipitation total for DJF computed over a 41-year study period. (b) Identified AR clusters labeled with AR event duration (blue), gap length duration (gray), and total AR cluster duration (red). (c) Histogram displaying distribution of storm total precipitation for all significant AR clusters recorded between 1979 and 2019 at PDX in DJF. The total accumulated precipitation, number of contributing AR events, and total duration per cluster is labeled in the corresponding table and noted on the histogram for context.

of timescales at BBY, up to about a month, implying the same string of ARs may be considered significantly clustered at one location and not another. For robustness, the false discovery rate procedure and significance requirements implemented here are relatively conservative. For example, when the observed K is compared against the average synthetic K, results show a systematically positive difference for all three locations (Figure S3 in Supporting Information S1), signifying that clustering occurs quite consistently, even when it does not meet the stringent statistical significance tests we imposed.

3.2. Winter Season Case Studies

We further examine precipitation timeseries for winter seasons with a high ratio of clustered ARs to total ARs at PDX, BBY, and LAX, to provide concrete examples of AR clustering and the associated impacts (Figures 3–5). Each DJF season is illustrated as a timeseries of AR events (blue shading; panel a), including hourly precipitation (black line) and integrated water vapor (IVT; blue line), to which the AR clustering framework is applied (panel b). Clusters are further contextualized based on the probability distribution of storm total precipitation among all wintertime AR clusters at the given location (panel c). For comparison, winter seasons with no identified clustering, displaying pronounced regularity or underdispersion in AR occurrence, are shown in Figure S4 in Supporting Information S1 for each location.

3.2.1. 1996/1997 Portland, Oregon

In the winter of 1996/1997, the Pacific Northwest (PNW) experienced several sequential heavy precipitation events yielding notable hydrologic impacts and associated damages on the order of $1 billion (CNRFC NOAA, 2000). Characterized by a shift in the overall weather pattern from a polar air mass to a warmer, wetter tropical regime, the melting December snowpack generated excessive January runoff. During this season, PDX experienced 11 AR

events, with several hourly precipitation totals exceeding the 95th percentile (Figure 3a), comprising four statistically significant AR clusters (Figure 3b). These clusters persisted for 6, 9, 14, and 6 days, respectively, containing 3, 3, 3, and 2 AR events, and producing 53, 308, 111, and 14 mm of precipitation. Based on the probability distribution of storm total precipitation among all wintertime AR clusters at PDX (Figure 3c), the 1996/1997 clusters span the full distribution. All clusters are below the 95th percentile, barring the second cluster, which is situated at the end of the distribution's right tail and contains hourly IVT maximum exceeding 1,000 kg m^{-1} s^{-1}.

3.2.2. 2016/2017 Bodega Bay, California

Northern California experienced a record wet water year in 2016/2017 associated with successive ARs. Among other impacts, the excessive runoff from snowpack over the Sierra Nevada damaged both the main and emergency spillways of the Oroville Dam, prompting the evacuation of over 188,000 people and over $1 billion in damages (Corringham et al., 2019). Based on the AR event definition applied here, 13 individual AR events occurred at BBY between December 2016 and February 2017, yielding several instances with hourly precipitation totals exceeding the 95th percentile (Figure 4a). Three AR clusters were identified, consisting of between 3 and 5 AR events each (Figure 4b). Like the PDX case (Figure 3), these clusters were equally distributed across the winter season. The shorter initial cluster persisted for just under a week, producing 190 mm of total precipitation. The latter two events each lasted ∼19 days, producing over 500 mm of precipitation each containing extremely intense AR events with IVT exceeding 1,000 kg m^{-1} s^{-1}. Relative to other AR-cluster precipitation totals at BBY, the first cluster was relatively minor, but the latter two produced precipitation totals falling just shy of the 95th percentile (Figure 4c). These results align well with other cases in which flooding is shown to not always occur in conjunction with the heaviest storm totals (e.g., Tuel & Martius, 2021b). Precipitation phase and antecedent surface conditions, such as soil saturation, evaporative demand, or vegetation, can also be important factors (e.g., Berghuijs et al., 2019). It is likely that the clustered nature of the ARs played a critical role in exacerbating these hydrological impacts.

3.2.3. 2004/05 Los Angeles, California

The winter of 2004/05 was a record setting wet season for Los Angeles County. According to the National Weather Service, this season was characterized by a relatively dry November and December before a series of major storms hit from the end of December onward (NWS, 2005). There were eight total AR events with intensities (i.e., event maximum hourly IVT) ranging between ∼250 and 600 kg m^{-1} s^{-1}, generating two statistically significant clusters with several exceedances of 95th percentile hourly precipitation (Figures 5a and 5b). The first cluster comprised four ARs over a 16-day period (Figure 5b) and generated >220 mm of precipitation (Figure 5a). Making landfall on already saturated ground, the final event in the cluster was characterized by roughly four straight days of AR conditions. This particular event has been linked to widespread flash flooding and landslides across Southern California (NWS, 2005), likely worsened by the antecedent conditions created by the three preceding ARs. This cluster has also been highlighted as producing a large fraction of the annual precipitation in Los Angeles, supporting insights that the majority of California's climatological precipitation is attributable to just a small number of ARs (Rutz et al., 2014). Occurring over 11 days in mid-February, the second cluster contained 3 AR events and generated 158 mm of precipitation. According to the distribution of AR cluster driven precipitation, this cluster produced slightly above average precipitation, whereas the first was just shy of the 95th percentile (Figure 5c).

3.3. Regional Patterns of Significant AR Clustering Timescales

The grid point-specific results from Figure 2 are consistent with regional patterns of significant clustering timescales (Figures 6 and 7). The fraction of seasons with significant clustering, shown as an average across 5-day aggregation period intervals, reveals the highest values in the 6–10-day range, with values universally >0.6 (Figure 6). As the aggregation period increases, a distinct pattern emerges at the 16–20-day interval with higher values over the southern half of the domain and lower values over the northern half. Above the 15-day timescale, most of Oregon, Washington, and Idaho show values below 0.5, with a broad minimum (0.1–0.2) across central Oregon and the Cascade Range extending into Washington (geographic features identified in Figure S5 in Supporting Information S1). Minima are also visible across the interior and along the lee side of mountain ranges. This is likely from infrequent AR intrusion due to water vapor depletion following orographic lift. Along the Coastal Ranges of the Southwest, a large majority (0.8) of seasons are significant out to the 15-day timescale. Values exceeding 0.5 persist across most of California out to 25 days. As aggregation periods increase, values exceeding 0.5 are confined to a small region just south of Cape Mendocino in Northern California out to 35 days and across parts of the Sierra Nevada out to 50 days.

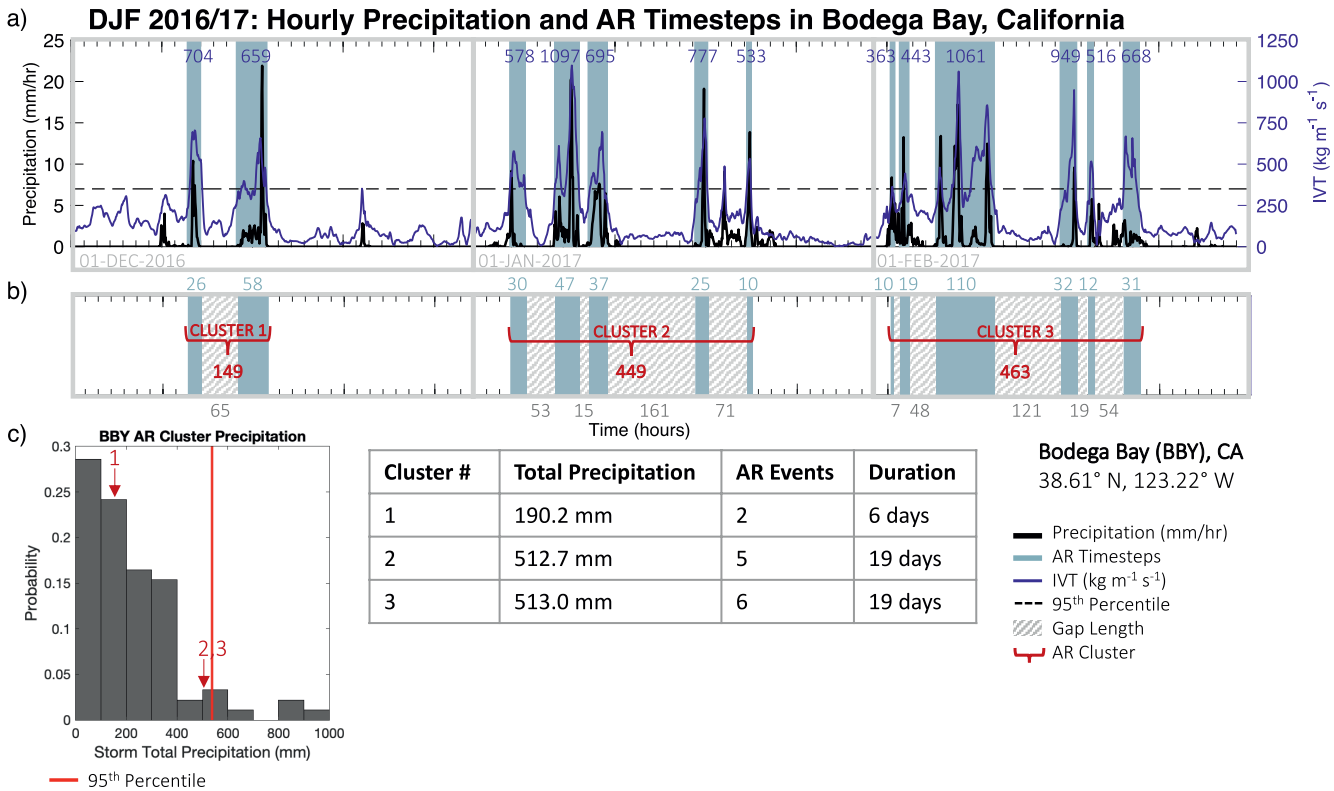

Cluster #	Total Precipitation	AR Events	Duration
1	190.2 mm	2	6 days
2	512.7 mm	5	19 days
3	513.0 mm	6	19 days

Figure 4. As in Figure 3, except for December 2016 through February 2017, at Bodega Bay, California.

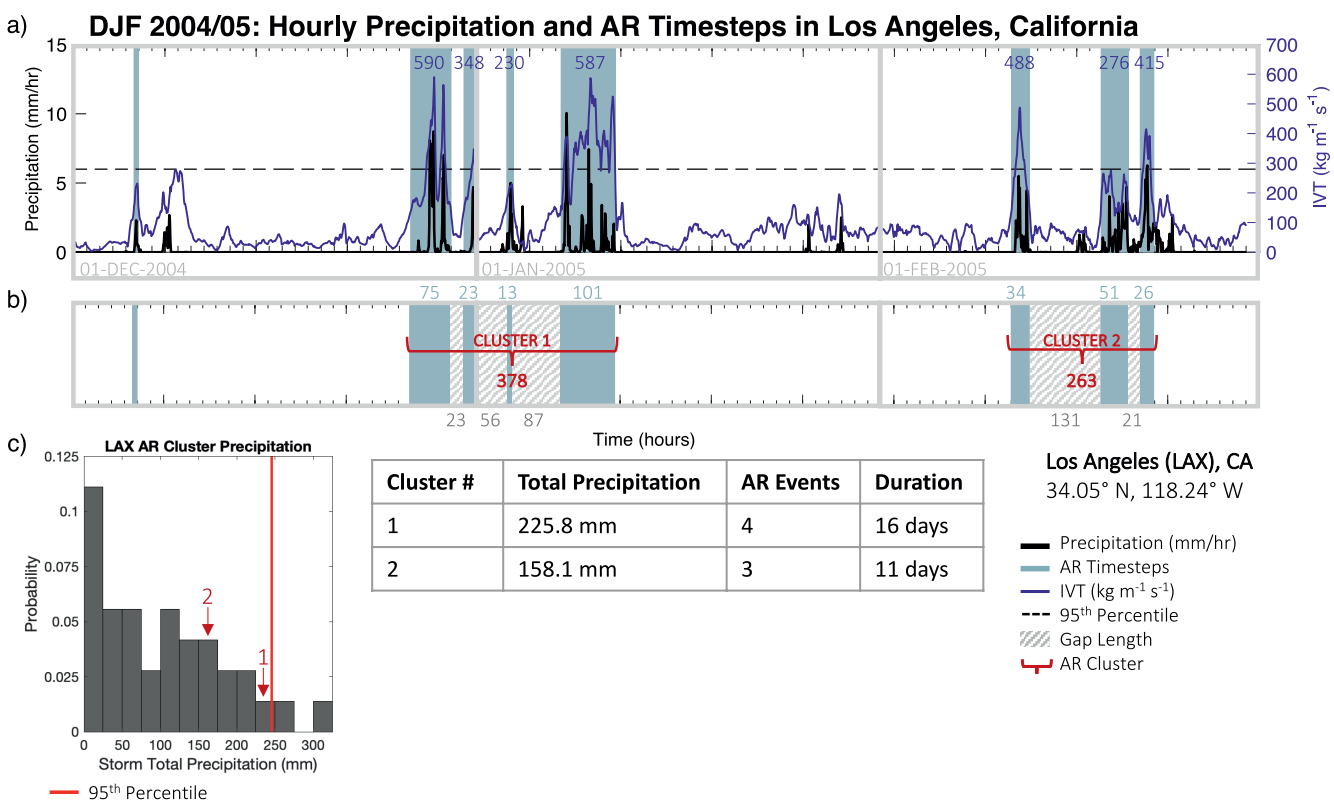

Cluster #	Total Precipitation	AR Events	Duration
1	225.8 mm	4	16 days
2	158.1 mm	3	11 days

Figure 5. As in Figure 3, except for 1 December 2004 through February 2005, at Los Angeles, California.

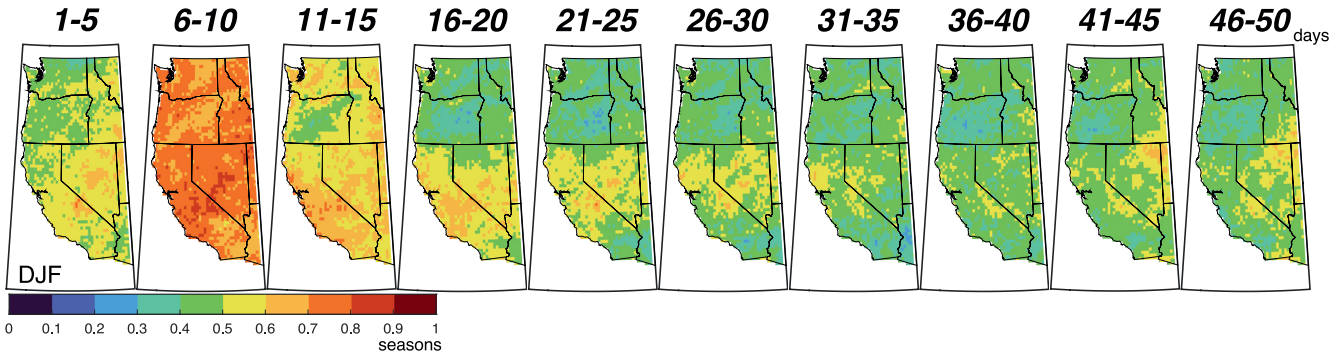

Figure 6. Average fraction of seasons with statistical significance across aggregation periods (days) at 5-day intervals at each grid point for DJF.

Patterns of the maximum aggregation periods with significance (Figure 7) are characterized by higher values across the South compared to the North. Values reaching the 50-day timescale are visible across the Sierra Nevada and portions of the northern California coast. Across Central and Southern California values range between 20 and 35 days. In contrast, Washington and coastal Oregon show significance out to 20 days. Central Oregon displays a broad minimum of less than 15 days. The absence of significant clustering across the PNW past the 15–20-day timescale occurs despite relatively high AR event occurrence during the winter months (Figure 1). Thus, ARs are frequent and randomly distributed once time intervals longer than a couple of weeks are considered. Significant clustering is seen over longer timescales across the Great Basin, which is characterized by a relatively lower AR occurrence (Figure 1). This indicates that although infrequent, when ARs do occur, they cluster together at a greater-than-random rate, for timescales out to ~35 days. Landfalling ARs in this region have been known to penetrate this far inland, although related precipitation is rare (Rutz et al., 2014). Broad consistency is found in the North/South patterns of short/long maximum aggregation periods using an alternative (i.e., fixed IVT threshold) AR detection algorithm (Figure S6b in Supporting Information S1). The greatest differences are apparent across portions of the interior where AR frequency characteristics are most uncertain (Figure S6a in Supporting Information S1).

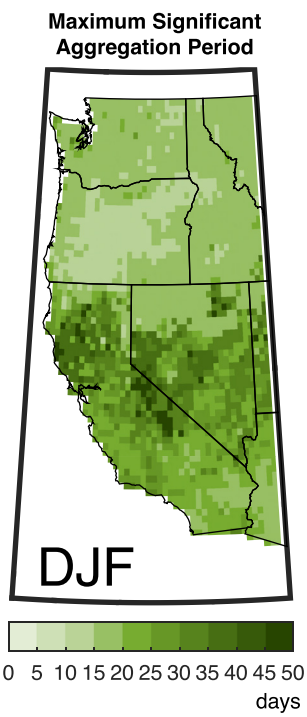

Figure 7. Maximum aggregation period (days) with statistically significant clustering for DJF at each grid point.

3.4. Characteristics of AR Clusters

3.4.1. AR Cluster Frequency

Having highlighted the timescales at which ARs are clustered across the western US, we proceed to analyze the climatological characteristics of western US AR clusters. AR cluster frequency (i.e., average clusters/season) is characterized by a maximum (>2/season) along the coast of Northern California south of Cape Mendocino (Figure 8a). Secondary maxima (>1.6/season) are visible across the Coast-Cascade Ranges of Oregon and Washington (Figure 8a). Minima (~0.5/season) in AR cluster frequency are found across lower elevations of Washington and Oregon. Across California, AR cluster frequency reveals a negative North-South gradient ranging from greater than 2 in the north, to 1.6 across the Central Valley, to between 1 and 1.2 across Southern California. Uncertainty in AR cluster frequency stemming from AR detection tool (ARDT) choice is provided in Figure S6c in Supporting Information S1. Algorithms tend to agree on areas of maximum clustering, with the largest disagreement found across the interior and southern portions of the domain likely due to differences in the algorithm's IVT threshold technique (i.e., relative vs. fixed).

Computed as the fraction of the total length of the season (Figure 8b), AR clusters (i.e., any time from the first timestep of first AR event in the cluster to the last timestep of the last AR event in the cluster, including the gap time between events) account for the largest fraction of time (30%) across portions of Northern California. Broad minima (5%–10%) are visible across

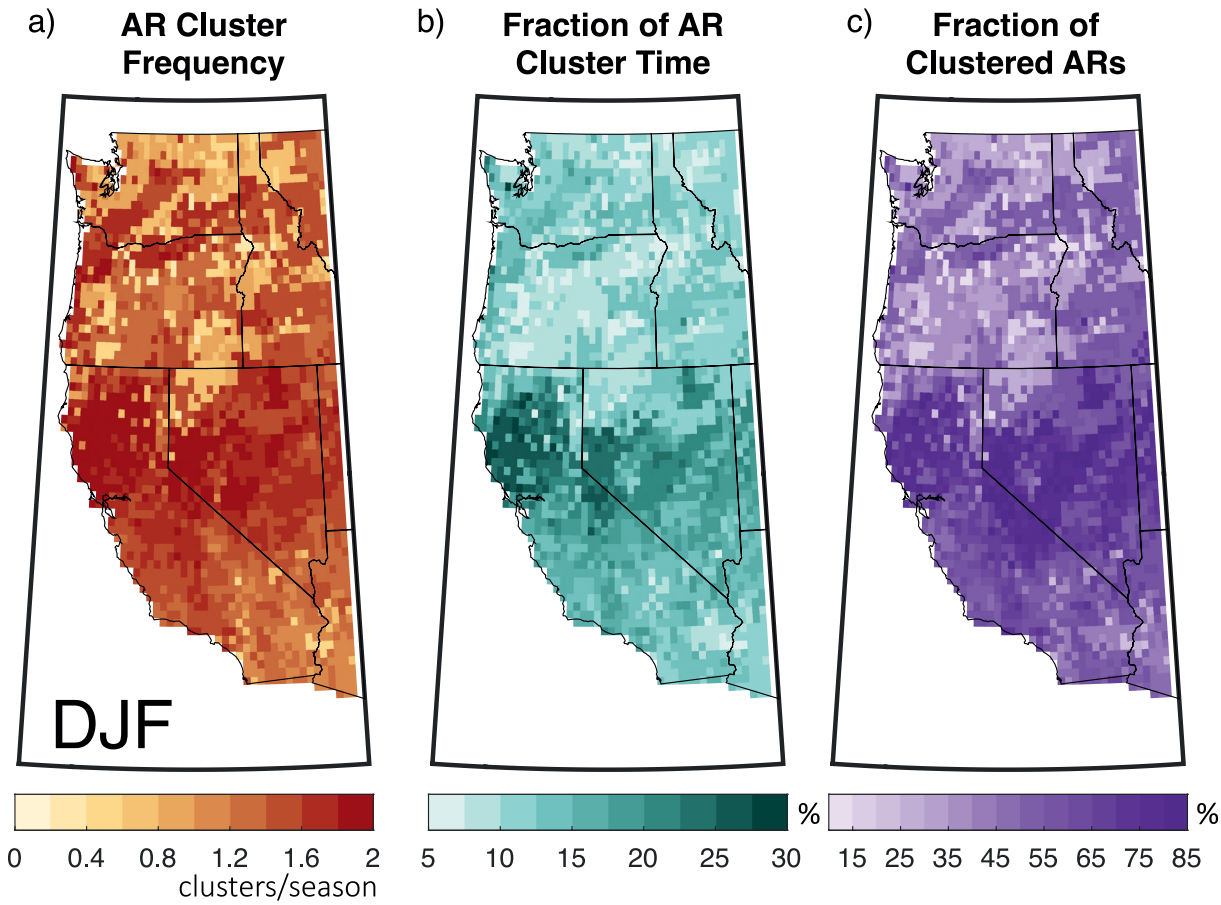

Figure 8. AR cluster frequency shown as (a) average clusters per season, (b) fraction (%) of time with AR cluster conditions, and (c) fraction (%) of total AR events that are clustered. Results are shown for DJF calculated at each grid point for 1979–2019.

the PNW, with slightly elevated values across the Coastal-Cascade Ranges (~15%). Less heterogeneity is apparent across Central and Southern California, where clustered events comprise 15%–20% of the season. While cluster frequency (Figure 8a) is influential here, similarities are also apparent between this pattern and that of the maximum aggregation periods with significance (Figure 4). Regions where ARs cluster at longer timescales (e.g., the Southwest) will naturally experience a greater amount of seasonal time under a cluster than regions where ARs cluster at shorter timescales (e.g., the Northwest).

The ratio of clustered AR events to total AR events (Figure 8c) displays a similar pattern to that of AR cluster frequency (Figure 8a). ARs occurring as a part of a cluster account for >85% of total AR occurrence along the coast of Northern California and in the Sierra Nevada. Elevated values are also found over the Central Valley of California and to the north along the Cascade Range and Olympic Peninsula (60%–70%). Values are generally lower (20%) across central Oregon and on the lee sides of the Olympic-Cascade Ranges of Washington. A high degree of correlation is apparent across all three frequency metrics (Figures 8a–8c), highlighting the northern half of California as the region where AR clusters are most common and comprise the greatest fraction of ARs. The southern half of California is a secondary center of action, followed by the PNW.

3.4.2. AR Cluster Duration and Contributing Events

Mean AR cluster duration is defined as the average number of hours of AR cluster conditions (including gaps) at a given location. The longest duration (>336 hr) clusters are found on the Olympic Peninsula, along the Coast-Cascade Ranges of Washington and across Northern California (Figure 9a). Comparatively, broad minima (<192 hr) reflecting shorter-lived clusters are apparent across Central Oregon and inland across portions of Idaho and northern Nevada. Across Central and Southern California values range from 192 to 198 hr, with a pocket of elevated values over the Transverse Range. Differences among regional patterns in Figure 4 versus Figure 9a

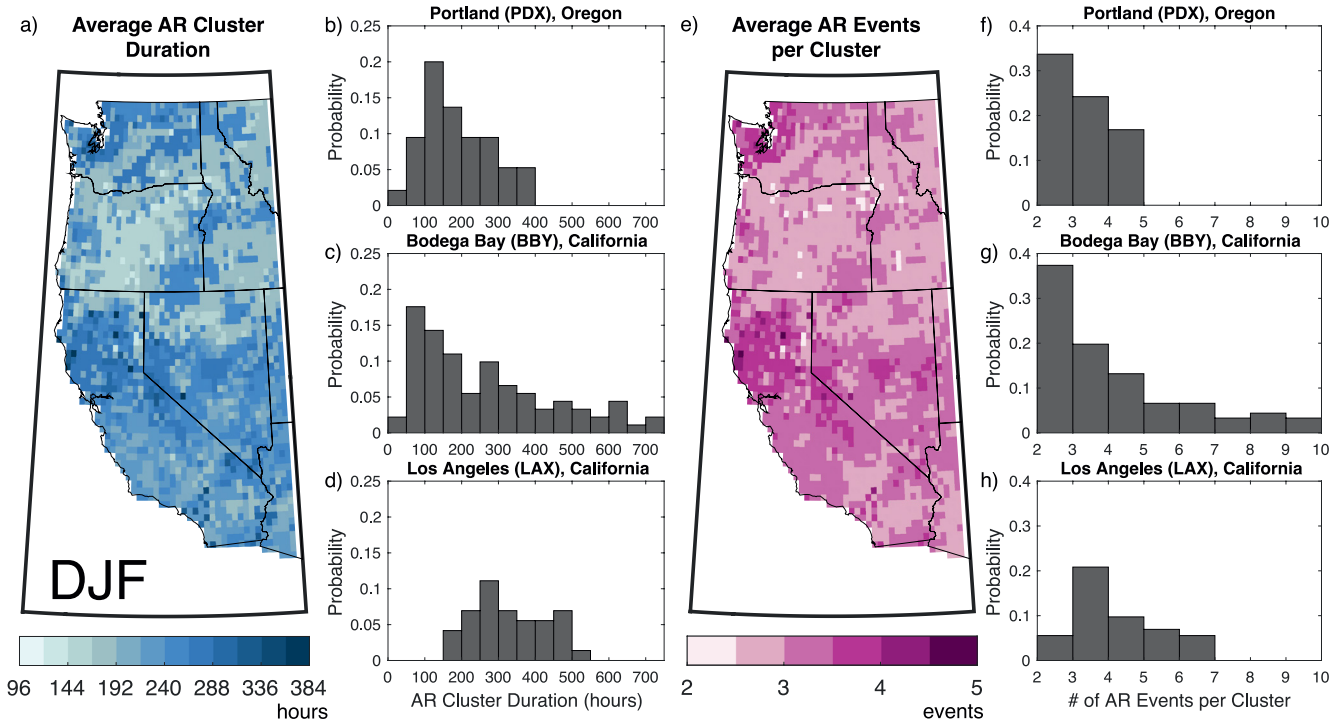

Figure 9. Average (a) AR cluster duration (hours; blue shading) and (e) AR event count per cluster (magenta shading) are shown at each grid point. Histograms of (b–d) AR cluster duration and (f–h) AR events per cluster at Portland, Oregon; Bodega Bay, California; and Los Angeles, California. Results are shown for DJF for 1979–2019.

(e.g., Washington) suggests maximum significant clustering timescales are not necessarily determinant of average cluster duration. Histograms of AR cluster duration for three select locations provide insight into why this might be the case, revealing substantial variability in the shape and spread of the duration distribution. At PDX (Figure 9b), AR clusters range from a few hours to just over two weeks in length, but most commonly persist for about a week. BBY has a much broader distribution, with a long right tail extending to over 700 hr or ~30 days in length. At LAX (Figure 9d), the distribution is relatively narrow with a higher degree of uniformity compared to the other locations. The shortest-lived clusters at this location are at least 150 hr in length but can last up to 500 hr or ~20 days. ARDT choice uncertainty surrounding average AR cluster duration is shown in Figure S6d in Supporting Information S1. Although some areas with longest-lived clusters are retained (e.g., Olympic Peninsula and Northern California), algorithms tend to diverge across portions of the interior.

Mean AR count per cluster refers to the average number of individual AR events contributing to a cluster at a given location (Figure 9e). Patterns align well with AR cluster duration (Figure 9a), indicating longer (shorter) duration clusters tend to be composed of a higher (lower) count of individual AR events. The maximum (5 AR events) is found on the northern California Coast just south of Cape Mendocino. Corridors of secondary maxima (4 AR events) are visible across Northern California and the Transverse Range of Southern California, as well as on the Olympic Peninsula along coastal Washington. AR clusters across Central California and the Washington Cascade Range tend to be composed of 3 AR events on average. Broad minima (<3 AR events) are found across central Oregon and the Northwest interior, as well as across portions of Southern California. Histograms indicate that AR clusters at PDX (Figure 9f) are composed of 2–4 AR events. A larger spread in the distribution at BBY (Figure 9g) is characterized by a long right-tail, indicating clusters can contain up to 9 individual AR events. A more uniform distribution at LAX (Figure 9h) shows clusters range between 2 and 6 AR events, with 3–4 events being the most common.

3.5. AR Cluster Precipitation

3.5.1. Fraction of Precipitation Associated With AR Clusters

We subsequently analyze AR cluster precipitation at a high spatial resolution based on the co-occurrence of AR clusters and 9-km precipitation data from ERA5-WRF. The fraction of AR cluster-driven precipitation is

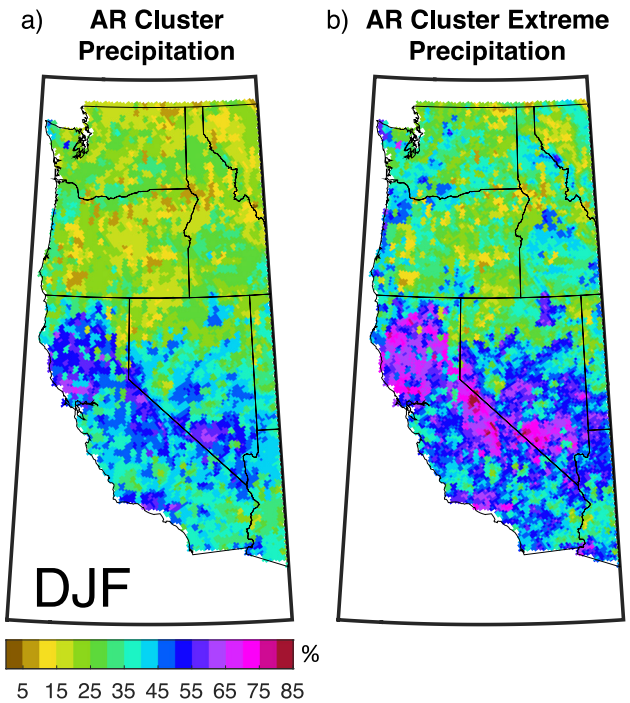

Figure 10. Fraction (%) of (a) total precipitation amount and (b) extreme precipitation occurrences (i.e., exceedance of the 95th percentile hourly precipitation shown in Figure S7 in Supporting Information S1) associated with AR clusters. Results are shown for DJF calculated at each grid point for 1979–2019.

largest (65%) across the coastal mountains of Northern California, over portions of the Sierra Nevada, and along the windward side of the Transverse Range (Figure 10a). There is a stark contrast between the fraction in the northern half of the domain compared to the southern half. Lower fractions (<35%) across the Northwest likely reflect shorter aggregation periods (10–15 days) with significance (Figure 4), yielding short-lived clusters (Figure 9a) accounting for a smaller proportion of total precipitation. ARs unassociated with significant clusters are likely responsible for the majority of wintertime precipitation in the PNW, while the opposite is true throughout most of California.

The extreme precipitation fraction (i.e., fraction of 95th percentile hourly precipitation totals associated with AR clusters; Figure 10b) follows a similar pattern to the precipitation fraction (Figure 10a) but with stronger gradients and a higher degree of spatial variability. Domain-wide 95th percentile hourly precipitation thresholds are illustrated in Figure S7 in Supporting Information S1 for context. The extreme precipitation fraction is largest (85%) over the northern extent of the Sierra Nevada. Secondary maxima (>65%) are visible across Northern California and the Transverse Range. Across the Northwest, larger values (50%) coincide with regions of complex terrain, including the Olympic Peninsula and Coast-Cascade Ranges, as well as portions of the Central Idaho Mountains. Minima (5%–25%) are found over regions of lower elevation across central Oregon and portions of the northern interior.

3.5.2. Interannual AR Cluster Characteristics

The interannual characteristics of AR clusters and associated precipitation for PDX, BBY, and LAX display a high degree of variability. At PDX (Figure 11a), the clustered events (gray bar) comprise all the AR events for several seasons including, 1997, 1998, 2011, and 2016. Years with a high ratio of clustered to total AR events also tend to be associated with unusually heavy precipitation. For example, the 1997 and 2016 seasons coincide with exceedances (black line) of the 95th percentile threshold (dashed line) for wintertime total precipitation accumulation which are mirrored by peaks in AR cluster-driven precipitation (red line). A detailed look into the 1997 winter season is provided in Figure 5. In 2016, all 11 AR events occurred as a part of a cluster, generating 500 mm of the 600 mm total accumulation for the season. Clustering accounts for 43% of the interannual variance in precipitation at PDX, despite the fact that AR clusters do not contribute to the majority of the precipitation at this location (Figure 10a).

At BBY (Figure 11b), a higher variation in the number of clustered AR events is apparent from year to year. As at PDX, the variation in the number of clustered AR events accounts for much of the variation in both the number of ARs themselves and the interannual variation in precipitation. The 1998 and 2017 winter seasons stand out as having total seasonal precipitation accumulations exceeding the 95th percentile. It is interesting that although the 1998 winter season had high AR occurrence, only a small percentage occurred as a part of a cluster. This is unlike the 2017 case (see Figure 6 for more detail), or indeed all other years except for 2000. The 1983 season is also notable with a precipitation total just shy of the 95th percentile, characterized by 17 clustered AR events responsible for a large proportion of the precipitation. Seasons with low AR event frequency and total precipitation, such as 1985 and 1989, reveal zero AR clusters. Overall, 28% of the interannual variance of total precipitation is explained by clustering at BBY, supporting their importance for water availability at this location.

The interannual distribution of AR events at LAX exhibits generally lower seasonal precipitation and AR frequency compared to the other locations, consistent with Figures 1a and 1c. Clustering is present for 26 of the 41 seasons analyzed, unlike the other locations where almost every season contains clusters. The 1993 and 1998 winter seasons have the highest total accumulated precipitation, both associated with 11 AR events, however only 1993 shows clustering, while 1998 shows no clustering, as at BBY. The 2017 season stands out as having the highest AR count of 18 events, 12 of which were clustered, generating ~400 mm of total precipitation with ~250 mm attributable to clustering. Several years show a strong presence of clustering coinciding with peaks in

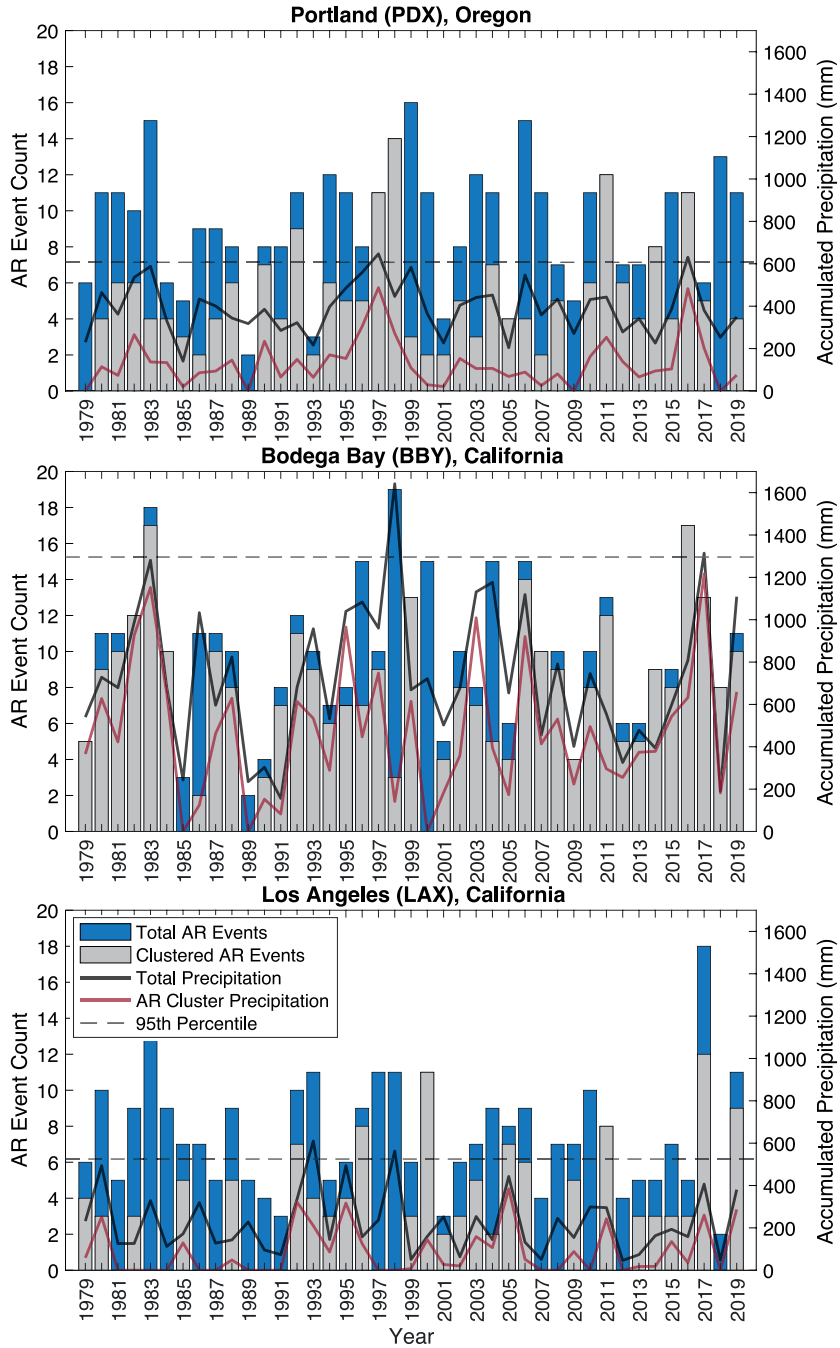

Figure 11. The distribution of AR events per year for DJF as total AR events (blue bars) and clustered AR events (gray bars). Interannual precipitation is shown as total accumulated seasonal precipitation per year (black line) and precipitation associated with AR clusters (red line). The dashed line reflects the 95th percentile of cumulative seasonal precipitation. Results are shown at (a) Portland, Oregon, (b) Bodega Bay, California, and (c) Los Angeles, California for 1979–2019.

the distribution of precipitation. The interannual variance of AR cluster driven precipitation accounts for 36% of the total precipitation variance at LAX.

4. Conclusions and Discussion

AR clusters are temporally compounding events consisting of extended periods of AR conditions and potentially devastating cumulative impacts. This study applies a novel statistical framework for quantifying subseasonal

temporal clustering to a 41-year (1979–2019) AR timeseries over the western US in DJF. Timescales in which clustering occurs preferentially over the historical record are determined based on a comparison between observed AR occurrence and a synthetic timeseries of random AR event occurrence. Results provide a definition for AR clustering alongside an evaluation of their climatological characteristics including, frequency, duration, and associated precipitation.

Here an AR cluster is defined as a sequence of AR events occurring over a statistically significant period of overdispersion (i.e., more clustered than expected due to chance). Across the western US, AR clusters display spatiotemporal variability in their characteristics constituting a distinct spatial pattern that separates the Northwest from the Southwest. Compared to simulations of random event occurrence, ARs are significantly clustered over shorter timescales in the Northwest (two weeks or less) but over a wider range of timescales in the Southwest (over a month in places) (Figures 6 and 7). For perspective, a case study analysis placing notable winter seasons within this statistical framework illustrates a coincidence with multiple clusters at three locations along the US West Coast (Figures 2–4). Cluster storm total precipitation for these events seldom exceeded the 95th percentile of all collocated cluster event accumulated precipitation. This suggests the outsized impacts of the events stem from antecedent surface conditions and land-surface interactions linked to the sequential nature of the events (e.g., soil saturation, evaporative demand, vegetation). How these effects may amplify AR cluster impacts deserves a more detailed investigation.

AR cluster frequency is largest (>2/season) over the northern Coastal Range of California (Figure 8a). In this region, clustering occurs >30% of the time (Figure 8b) and accounts for ∼85% of total AR occurrence (Figure 8c). These clusters are characterized by long durations (up to a month) composed of high individual AR counts (∼5 AR events; Figure 9b). Long-lived clusters are also found across the Transverse Range, a region dependent on just a few ARs for the majority of its annual precipitation (Dettinger et al., 2011; Neiman et al., 2013). Clustering is less frequent across portions of Oregon and Washington. Here clusters account for a smaller fraction of time in DJF (∼15%), constituting roughly 50% of total AR occurrence, suggesting that a large proportion of ARs are occurring independently or over timescales not considered significant by Ripley's K. High cluster frequency visible in Washington follows a northeast-southwest orientation collocated with the Cascade Range (Figures 8a and 8c). The increased presence of clustering over portions of the interior domain may be related to inland/interior penetrating ARs which tend to have a more amplified flow pattern compared to coastal-decaying ARs (Rutz et al., 2015).

AR's clustering more than what would be expected by chance suggests dynamical mechanisms favor cluster development. Although outside the scope of this study, longer versus shorter clustering durations may be driven by differing meteorological environments and/or mechanisms, which may have implications for their predictability (Fish et al., 2022). Long duration clustering among ETCs has been linked to persistent large-scale flow patterns and their interaction with successive Rossby wave-breaking patterns (Dacre & Pinto, 2020). Shorter duration sequences composed of fewer AR events may be characterized by different synoptic environments (e.g., mesoscale frontal waves or migratory eddies) (Fish et al., 2019; Nakamura, 1992; Nakamura & Sampre, 2002). Amplified flow patterns associated with interior penetrating ARs (i.e., more southwesterly flow (vs. westerly) and larger water vapor transport than coastal decaying ARs; see Rutz et al., 2015) may be favorable to a cluster of ARs that are sufficiently strong/moist to penetrate and be detected over interior/leeside regions. The distinct statistically significant clustering timescales presented here can be leveraged to investigate the dynamics and synoptic environments that favor AR cluster development for improved predictability and situational awareness.

As expected, the contribution of AR cluster-related precipitation, represented by the fractions of total (55%–65%) and extreme precipitation (70%–85%) (Figure 10), is largest over Northern California, along the Sierra Nevada, and across the Transverse Range. This result is consistent with the spatial pattern of average total precipitation accumulation for AR family events over California in Fish et al., 2022, displaying higher values collocated with areas of enhanced topography. Less precipitation is attributable to clustering across the PNW (≤35%), suggesting a larger contribution from ARs that are randomly distributed in time and/or a role for other precipitation-generating mechanisms (e.g., closed lows; see Abatzoglou, 2016). Alternatively, lower fractions across portions of the Northwest interior and Great Basin likely reflect water vapor depletion due to orographic precipitation processes (e.g., Smith et al., 2005, 2010) resulting in fewer, less moisture laden ARs further inland. The contrasting north-south pattern is attributable to the relatively shorter timescales at which ARs significantly cluster in the north. AR clusters display large interannual variability across winter seasons (Figure 11). Histograms of AR cluster frequency

and associated precipitation over 41 winter seasons suggest AR clusters may be responsible for modulating wet versus dry years consistent with Fish et al., 2022 and AR family frequency characteristics during active/inactive water years. This is particularly true farther south where the presence/absence of a single cluster may drastically alter the annual precipitation.

Although the statistical framework applied here is intuitive, it has its limitations. Significance testing requiring the majority of years and aggregation periods within each 5-day interval to have significance reflects a high degree of stringency. Less conservative requirements would have the potential to produce a higher occurrence of clustering, accounting for a higher proportion of the interannual variance of total precipitation. These results are somewhat sensitive to the gap length (i.e., ≤10 days) chosen to define AR strings prior to filtering against the Ripley's K output. A narrower gap length definition requiring fewer timesteps (i.e., ≤5 days) between individual AR events would result in a higher count of shorter duration clusters but would not largely change the fraction of AR cluster time per season. Sensitivity to ARDT choice indicates uncertainty in AR cluster characteristics when comparing relative versus fixed IVT threshold techniques (Figure S6 in Supporting Information S1). Broad consistency was found in areas where AR clusters are most frequent and long-lived (Figures S6c and S6d in Supporting Information S1). Algorithm disagreement was most apparent across the drier interior where AR event frequency is most uncertain (Figure S6a in Supporting Information S1). Permissive ARDTs (e.g., Guan & Waliser, 2015) detect non-traditional AR shapes that can influence spatial patterns of AR cluster metrics (e.g., high spatial variability across Washington in Figures 8a and 8c). The spatiotemporal progression of large AR features with appendages can lead to persistence and breaks (i.e., noise) in AR conditions at a grid point contributing to heterogeneity among AR cluster climatologies. Ultimately, the main conclusions relating to the distinctions between the Northwest and California would be qualitatively similar and robust to the methodological choices discussed above.

Results from this analysis aim to improve our understanding of the characteristics and impacts associated with multiple sequential ARs affecting the western US. This largely understudied topic has important ramifications for the occurrence of megaflood events, such as ARkstorm, as well as drought, which pose a significant ecological and socioeconomic threat. More broadly, changing spatiotemporal patterns of extended periods of AR conditions (i.e., cluster duration) are critical for improved situational awareness informing AR predictability and forecasting. As a historical analysis, results are intended to serve as a benchmark for measuring future change in AR clustering under warming. We also plan to extend this methodology geographically to characterize spatiotemporal patterns of AR clustering globally. Although outside the scope of this study, dynamical mechanisms acting on longer temporal and spatial scales than AR events, such as Rossby wave breaking and North Pacific jet dynamics, have been shown to foster AR and cyclone development (Griffin & Martin, 2017; Hu et al., 2017; Mundhenk et al., 2016). Future work examining the primary synoptic environments and potential AR/ETC cluster co-occurrence has the potential to improve our understanding of AR cluster formation and the dynamics driving heavy precipitation and flooding. With warming likely to induce change, a robust understanding of the tendency of ARs to cluster in time and space is imperative to mitigate risk and inform effective adaptation strategies.

Data Availability Statement

All AR data are available from the Climate Data Gateway (ARTMIP, 2022). WRF outputs are available on Amazon S3 and are accessible with Amazon Web Services Command Line Interface (AWS CLI, 2022). See https://registry.opendata.aws/wrf-cmip6/ for data access information. ERA5 data is available from the Copernicus Climate Change Service (C3S) Climate Data Store at https://cds.climate.copernicus.eu/ (Hersbach et al., 2023).

Acknowledgments
This work was funded by the US. Department of Energy, Office of Science, projects "A Framework for Improving Analysis and Modeling of Earth System and Intersectoral Dynamics at Regional Scales" and "Identifying Hydrologic Cycle Changes Under Future Climate" (award no. DE-SC0016605). We thank Stefan Rahimi for his help with the ERA5-WRF precipitation estimates. Conversations with David Neelin and Alan Rhoades also helped mature the statistical clustering framework.

References

Abatzoglou, J. T. (2016). Contribution of cutoff lows to precipitation across the United States. *Journal of Applied Meteorology and Climatology*, *55*(4), 893–899. https://doi.org/10.1175/JAMC-D-15-0255.1

ARTMIP. (2022). Atmospheric river tracking method intercomparison project: ARTMIP Tier 2 catalogues ERA5 reanalysis [Dataset]. Climate Data Gateway at NCAR. Retrieved from https://www.earthsystemgrid.org/dataset/ucar.cgd.artmip.tier2.catalogues.era5.html

AWS CLI. (2022). AWS S3 explorer: Wrf-cmip6_noversioning/downscaled_products/reanalysis/era5/hourly [Dataset]. Amazon Web Services Command Line Interface (AWS CLI). Retrieved from https://wrf-cmip6-noversioning.s3.amazonaws.com/index.html#downscaled_products/reanalysis/era5/hourly/

Barton, Y., Giannakaki, P., Waldow, H. V., Chevalier, C., Pfahl, S., & Martius, O. (2016). Clustering of regional-scale extreme precipitation events in southern Switzerland. *Monthly Weather Review*, *144*(1), 347–369. https://doi.org/10.1175/MWR-D-15-0205.1

Berghuijs, W. R., Harrigan, S., Molnar, P., Slater, L. J., & Kirchner, J. W. (2019). The relative importance of different flood-generating mechanisms across Europe. *Water Resources Research*, *55*(6), 4582–4593. https://doi.org/10.1029/2019WR024841

California Nevada River Forecast Center (CNRFC) NOAA. (2000). Heavy precipitation event: Southwest Oregon, Northern California, and Western Nevada: December 26, 1996 - January 3, 1997. Retrieved from https://www.cnrfc.noaa.gov/storm_summaries/jan1997storms.php

Cordeira, J. M., Ralph, F. M., & Moore, B. J. (2013). The development and evolution of two atmospheric rivers in proximity to western North Pacific tropical cyclones in October 2010. *Monthly Weather Review*, *141*(12), 4234–4255. https://doi.org/10.1175/MWR-D-13-00019.1

Corringham, T. W., Ralph, F. M., Gershunov, A., Cayan, D. R., & Talbot, C. A. (2019). Atmospheric rivers drive flood damages in the western United States. *Science Advances*, *5*(12). https://doi.org/10.1126/sciadv.aax4631

Dacre, H. F., & Pinto, J. G. (2020). Serial clustering of extratropical cyclones: A review of where, when and why it occurs. *npj Climate. Atmos. Sci.*, *3*(1), 48. https://doi.org/10.1038/s41612-020-00152-9

Dettinger, M. D., & Ingram, B. L. (2013). The coming megastorms. *Scientific American*, *308*(1), 64–71. https://doi.org/10.1038/scientificamerican0113-64

Dettinger, M. D., RalphDas, F. M. T., Neiman, P. J., & Cayan, D. R. (2011). Atmospheric rivers, floods, and the water resources of California. *Water*, *2011*(3), 445–478. https://doi.org/10.3390/w3020445

Dominguez, F., Dall'erba, S., Huang, S., Avelino, A., Mehran, A., Hu, H., et al. (2018). Tracking an atmospheric river in a warmer climate: From water vapor to economic impacts. *Earth System Dynamics*, *9*(1), 249–266. https://doi.org/10.5194/esd-9-249-2018

Fish, M. A., Done, J. M., Swain, D. L., Wilson, A. M., Michaelis, A. C., Gibson, P. B., & Ralph, F. M. (2022). Large-scale environments of successive atmospheric river events leading to compound precipitation extremes in California. *Journal of Climate*, *35*(5), 1515–1536. https://doi.org/10.1175/JCLI-D-21-0168.1

Fish, M. A., Wilson, A. M., & Ralph, F. M. (2019). Atmospheric river families: Definition and associated synoptic conditions. *Journal of Hydrometeorology*, *20*(10), 2091–2108. https://doi.org/10.1175/JHM-D-18-0217.1

Griffin, K. S., & Martin, J. E. (2017). Synoptic features associated with temporally coherent modes of variability of the North Pacific jet stream. *Journal of Climate*, *30*(1), 39–54. https://doi.org/10.1175/JCLI-D-15-0833.1

Guan, B., & Waliser, D. E. (2015). Detection of atmospheric rivers: Evaluation and application of an algorithm for global studies. *Journal of Geophysical Research: Atmospheres*, *120*(24), 12514–12535. https://doi.org/10.1002/2015JD024257

Guan, B., Waliser, D. E., & Ralph, F. M. (2018). An intercomparison between reanalysis and dropsonde observations of the total water vapor transport in individual atmospheric rivers. *Journal of Hydrometeorology*, *19*(2), 321–337. https://doi.org/10.1175/JHM-D-17-0114.1

Guirguis, K., Gershunov, A., Clemesha, R. E. S., Shulgina, T., Subramanian, A. C., & Ralph, F. M. (2018). Circulation drivers of atmospheric rivers at the North American west coast. *Geophysical Research Letters*, *45*(22), 12576–12584. https://doi.org/10.1029/2018GL079249

Hersbach, H., Bell, B., Berrisford, P., Biavati, G., Horányi, A., Muñoz Sabater, J., et al. (2023). ERA5 hourly data on single levels from 1940 to present [Dataset]. Copernicus Climate Change Service (C3S) Climate Data Store (CDS). https://doi.org/10.24381/cds.adbb2d47

Hersbach, H., Bell, B., Berrisford, P., Hirahara, S., Horányi, A., Muñoz-Sabater, J., et al. (2020). The ERA5 global reanalysis. *Quarterly Journal of the Royal Meteorological Society*, *146*(730), 1999–2049. https://doi.org/10.1002/qj.3803

Hu, H., Dominguez, F., Wang, Z., Lavers, D. A., Zhang, G., & Ralph, F. M. (2017). Linking atmospheric river hydrological impacts on the U.S. West Coast to Rossby wave breaking. *Journal of Climate*, *30*(9), 3381–3399. https://doi.org/10.1175/JCLI-D-16-0386.1

Huang, X., & Swain, D. L. (2022). Climate change is increasing the risk of a California megaflood. *Science Advances*, *8*(32). https://doi.org/10.1126/sciadv.abq0995

Kopp, J., Rivoire, P., Ali, S. M., Barton, Y., & Martius, O. (2021). A novel method to identify sub-seasonal clustering episodes of extreme precipitation events and their contributions to large accumulation periods. *Hydrology and Earth System Sciences*, *25*(9), 5153–5174. https://doi.org/10.5194/hess-25-5153-2021

Lamjiri, M. A., Dettinger, M. D., Ralph, F. M., & Guan, B. (2017). Hourly storm characteristics along the U.S. West Coast: Role of atmospheric rivers in extreme precipitation. *Geophysical Research Letters*, *44*(13), 11456–11462. https://doi.org/10.1002/2017GL075399

Mailier, P., Stephenson, D., Ferro, C., & Hodges, K. I. (2006). Serial clustering of extratropical cyclones. *Monthly Weather Review*, *134*(8), 2224–2240. https://doi.org/10.1175/mwr3160.1

Martius, O., Sodemann, H., Joos, H., Pfahl, S., Winschall, A., Croci-Maspoli, M., et al. (2013). The role of upper-level dynamics and surface processes for Pakistan flood of July 2010. *Quarterly Journal of the Royal Meteorological Society*, *139*(676), 1780–1797. https://doi.org/10.1002/qj.2082

Michaelis, A. C., Gershunov, A., Weyant, A., Fish, M. A., Shulgina, T., & Ralph, F. M. (2022). Atmospheric river precipitation enhanced by climate change: A case study of the storm that contributed to California's Oroville Dam crisis. *Earth's Future*, *10*(3), e2021EF002537. https://doi.org/10.1029/2021EF002537

Mundhenk, B. D., Banks, E. A., & Maloney, E. D. (2016). All-season climatology and variability of atmospheric river frequencies over the North Pacific. *Journal of Climate*, *29*(13), 4885–4903. https://doi.org/10.1175/JCLI-D-15-0655.1

Nakamura, H. (1992). Midwinter suppression of baroclinic wave activity in the Pacific. *Journal of the Atmospheric Sciences*, *49*(17), 1629–1642. https://doi.org/10.1175/1520-0469(1992)049<1629:MSOBWA>2.0.CO;2

Nakamura, H., & Sampre, T. (2002). Trapping of synoptic-scale disturbances into the North-Pacific subtropical jet core in midwinter. *Geophysical Research Letters*, *29*(16), 1761. https://doi.org/10.1029/2002GL015535

National Weather Service (NWS) Los Angeles/Oxnard CA. (2005). Public Information Statement: The second wettest rainfall season in Los Angeles has come to an end. Retrieved from http://www.sierraphotography.com/wxnotes/wxdata0405/nws_pnslox_070105_0420pdt.htm

Neiman, P. J., Ralph, F. M., Moore, B. J., Hughes, M., Mahoney, K. M., Cordeira, J. M., & Dettinger, M. D. (2013). The landfall and inland penetration of a flood-producing atmospheric river in Arizona. Part I: Observed synoptic-scale, orographic, and hydrometeorological characteristics. *Journal of Hydrometeorology*, *14*(2), 460–464. https://doi.org/10.1175/jhm-d-12-0101.1

Null, J., & Hulbert, J. (2007). California washed away: The great flood of 1862. *Weatherwise*, *60*(1), 26–30. https://doi.org/10.3200/WEWI.60.1.26-30

Payne, A. E., & Magnusdottir, G. (2014). Dynamics of landfalling atmospheric rivers over the North Pacific in 30 years of MERRA reanalysis. *Journal of Climate*, *27*(18), 7133–7150. https://doi.org/10.1175/jcli-d-14-00034.1

Pinto, J. G., Gomara, I., Masato, G., Dacre, H. F., Woollings, T., & Caballero, R. (2014). Large-scale dynamics associated with clustering of extratropical cyclones affecting Western Europe. *Journal of Geophysical Research: Atmospheres*, *119*(24), 13704–13719. https://doi.org/10.1002/2014JD022305

Porter, K., & Coauthors (2011). Overview of the ARkStorm scenario. U.S. Geological Survey Open-File Report 2010-1312, p 183 and appendixes. Retrieved from http://pubs.usgs.gov/of/2010/1312/

Priestley, M. D. K., Pinto, J. G., Dacre, H. F., & Shaffrey, L. C. (2017). The role of cyclone clustering during the stormy winter of 2013/2014. *Weather*, *72*(7), 187–192. https://doi.org/10.1002/wea.3025

Rahimi, S., Krantz, W., Lin, Y.-H., Bass, B., Goldenson, N., Hall, A., et al. (2022). Evaluation of a reanalysis-driven configuration of WRF4 over the western United States from 1980 to 2020. *Journal of Geophysical Research: Atmospheres*, *127*(4), e2021JD035699. https://doi.org/10.1029/2021JD035699

Ralph, F. M., Coleman, T., Neiman, P. J., Zamora, R. J., & Dettinger, M. D. (2013). Observed impacts of duration and seasonality of atmospheric-river landfalls on soil moisture and runoff in coastal northern California. *Journal of Hydrometeorology*, *14*(2), 443–459. https://doi.org/10.1175/jhm-d-12-076.1

Ralph, F. M., Rutz, J. J., Cordeira, J. M., Dettinger, M., Anderson, M., Reynolds, D., et al. (2019). A scale to characterize the strength and impacts of atmospheric rivers. *Bulletin America Meteorology Social*, *100*(2), 269–289. https://doi.org/10.1175/BAMS-D-18-0023.1

Ripley, B. D. (1981). *Spatial Statistics, Wiley series in probability and statistics*. John Wiley & Sons, Inc. https://doi.org/10.1002/0471725218

Rutz, J. J., Steenburgh, W. J., & Ralph, F. M. (2014). Climatological characteristics of atmospheric rivers and their inland penetration over the western United States. *Monthly Weather Review*, *142*(2), 905–921. https://doi.org/10.1175/MWR-D-13-00168.1

Rutz, J. J., Steenburgh, W. J., & Ralph, F. M. (2015). The inland penetration of atmospheric rivers over western North America: A Lagrangian analysis. *Monthly Weather Review*, *143*(5), 1924–1944. https://doi.org/10.1175/MWR-D-14-00288.1

Slinskey, E. A., Loikith, P. C., Waliser, D. E., Guan, B., & Martin, A. (2020). A climatology of atmospheric rivers and associated precipitation for the seven U.S. National Climate Assessment regions. *Journal of Hydrometeorology*, *21*(11), 2439–2456. https://doi.org/10.1175/JHM-D-20-0039.1

Smith, B. L., Yuter, S. E., Neiman, P. J., & Kingsmill, D. E. (2010). Water vapor fluxes and orographic precipitation over northern California associated with a landfalling atmospheric river. *Monthly Weather Review*, *138*(1), 74–100. https://doi.org/10.1175/2009mwr2939.1

Smith, R. B., Barstad, I., & Bonneau, L. (2005). Orographic precipitation and Oregon's climate transition. *Journal of the Atmospheric Sciences*, *62*(1), 177–191. https://doi.org/10.1175/jas-3376.1

Tuel, A., & Martius, O. (2021a). A climatology of sub-seasonal temporal clustering of extreme precipitation in Switzerland and its impacts. *Natural Hazards and Earth System Sciences*, *21*(10), 2949–2972. https://doi.org/10.5194/nhess-21-2949-2021

Tuel, A., & Martius, O. (2021b). A global perspective on the sub-seasonal clustering of precipitation extremes. *Weather and Climate Extremes*, *33*, 100348. https://doi.org/10.1016/j.wace.2021.100348

Tuel, A., & Martius, O. (2022). Subseasonal temporal clustering of extreme precipitation in the Northern Hemisphere: Regionalization and physical drivers. *Journal of Climate*, *35*(11), 3537–3555. https://doi.org/10.1175/JCLI-D-21-0562.1

Vano, J. A., Dettinger, M., Cifelli, R., Curtis, D., Dufour, A., Miller, K., et al. (2018). Hydroclimatic extremes as challenges for the water management community: Lessons from Oroville Dam and Hurricane Harvey. *Bulletin America Meteorology Social*, *100*(1), S9–S14. https://doi.org/10.1175/BAMS-D-18-0219.1

Villarini, G., Smith, J. A., Baeck, M. L., Vitolo, R., Stephenson, D. B., & Krajewski, W. (2011). On the frequency of heavy rainfall for the Midwest of the United States. *Journal of Hydrology*, *400*(1–2), 103–120. https://doi.org/10.1016/j.jhydrol.2011.01.027

Vitolo, R., Stephenson, D. B., Cook, I. M., & Mitchell-Wallace, K. (2009). Serial clustering of intense European storms. *Meteorologische Zeitschrift*, *18*(4), 411–424. https://doi.org/10.1127/0941-2948/2009/0393

White, A. B., Moore, B. J., Gottas, D. J., & Neiman, P. J. (2019). Winter storm conditions leading to excessive runoff above California's Oroville dam during January and February 2017. *Bulletin America Meteorology Social*, *100*(1), 55–70. https://doi.org/10.1175/BAMS-D-18-0091.1

Wilks, D. S. (2016). "The stippling shows statistically significant grid points": How research results are routinely overstated and overinterpreted, and what to do about it. *Bulletin America Meteorology Social*, *97*(12), 2263–2273. https://doi.org/10.1175/BAMS-D-15-00267.1

Zhu, Y., & Newell, R. E. (1998). A proposed algorithm for moisture fluxes from atmospheric rivers. *Monthly Weather Review*, *126*(3), 725–735. https://doi.org/10.1175/1520-0493(1998)126<0725:APAFMF>2.0.CO;2

Zscheischler, J., Martius, O., Westra, S., Bevacqua, E., Raymond, C., Horton, R. M., et al. (2020). A typology of compound weather and climate events. *Nature Reviews Earth & Environment*, *1*(7), 333–347. https://doi.org/10.1038/s43017-020-0060-z

Zscheischler, J., Westra, S., van den Hurk, B. J. J. M., Seneviratne, S. I., Ward, P. J., Pitman, A., et al. (2018). Future climate risk from compound events. *Nature Climate Change*, *8*(6), 469–477. https://doi.org/10.1038/s41558-018-0156-3